

High Strength Wood-based Sandwich Panels Reinforced with Fiberglass and Foam

Jinghao Li,^{a,b} John F. Hunt,^{b,*} Shaoqin Gong,^a and Zhiyong Cai^{b,*}

Mechanical analysis is presented for new high-strength sandwich panels made from wood-based phenolic impregnated laminated paper assembled with an interlocking tri-axial ribbed core. Four different panel configurations were tested, including panels with fiberglass fabric bonded to both outside faces with self-expanding urethane foam used to fill the ribbed core. The mechanical behaviors of the sandwich panels were strength tested *via* flatwise compression, edgewise compression, and third-point load bending. Panels with fiberglass exhibited significantly increased strength and apparent MOE in edgewise compression and bending, but there were no noticeable effects in flatwise compression. The foam provided improved support that resisted both rib buckling and face buckling for both compression and bending tests. Post-failure observation indicated that core buckling dominated the failures for all configurations used. It is believed that using stiffer foam or optimizing the dimension of the core might further improve the mechanical performance of wood-based sandwich panels.

Keywords: Wood-based Laminate paper; Foams; Glass fibers; Sandwich structure; Mechanical testing

Contact information: a: Department of Biomedical Engineering, Wisconsin Institutes for Discovery, and Materials Science and Program, University of Wisconsin-Madison, 330 North Orchard Street, Madison, WI 53715 USA; b: USDA Forest Service, Forest Products Laboratory, One Gifford Pinchot Drive, Madison, WI 53726 USA; *Corresponding authors: jfhunt@fs.fed.us; zcai@fs.fed.us

INTRODUCTION

Sandwich panels are used for a variety of structural applications, including building construction, transportation, decking, marine, and aerospace (Davalos *et al.* 2001; Li *et al.* 2013; Sharaf and Fam 2011; Vasiliev *et al.* 2001; Wei *et al.* 2013). Design efficiencies for optimum performance, especially to obtain a high strength-to-weight ratio, are achieved by optimizing the geometry and orientation of materials used for the faces and core. Many sandwich panels are fabricated using foam or honeycomb construction as the core structure. However, over the past 15 years, research has demonstrated that a new interlocking composite grid arrangement could offer improved performance for some applications, particularly for large civil structures (Han and Tsai 2003; Chen and Tsai 1996). This interlocking grid uses linear ribs that are double slotted 1/3 from each edge across the width or single slotted 2/3 from one edge across the width of the rib. In this study, ribs that were double notched were used as the main rib oriented along the length of the panels, and the 2/3 notched ribs were inserted from either the top or bottom sides at a 60-degree angle to create a tri-axial core design, as shown in Fig. 1 (Li *et al.* 2013). For some applications, this core configuration has been shown to be stiffer and stronger than foam and honeycomb core at the same cost, using a specific density assumption (Evans *et al.* 2001; Zhang *et al.* 2008). The equilateral-triangle design

can be easily modified by adjusting the distance between slots or changing the design to an isosceles triangle, for example, by adjusting the distance between slots for the double-slotted ribs.

The Forest Products Laboratory (FPL) is working to develop 3D engineered sandwich panels made from wood-based composites that can be engineered to have specific performance with low cost for a variety of applications. For some applications, such as marine or aerospace, high performance, low weight, and water resistance are required. However, for other panels, such as building construction materials or furniture, the high-performance requirements for low weight and water resistance are not necessary and introduce additional costs. There are materials such as phenolic impregnated laminated paper that might be sufficient to fill other less demanding applications. Phenolic impregnated laminated paper was used in this study to fabricate the rib components and for the initial top and bottom faces. The laminated paper was selected based on its higher strength and water resistant properties compared with fiberboard or paper (Hunt *et al.* 2004).

Fiber-reinforced plastics (FRPs) have been commonly used as reinforcing materials and structures (Plevris and Triantafillou 1992, Johnsson 2006); they generally yield higher performance and strength properties than those without reinforcement. Specific reinforcements are targeted to enhance specific performance attributes. For example, in a previous study (Li *et al.* 2013), improved panel bending performance was demonstrated when carbon fiber fabric was bonded to either side. Research has also shown that foam can be used to prevent face buckling in edgewise compression and rib buckling for cores in flatwise compression, especially in sandwich panel with thin thickness (Taczala and Banasiak 2004). In addition, the degree of foam stiffness has been shown to improve compression strength (Aviles and Carlsson 2006).

Researchers have also investigated the mechanical properties of sandwich panels using lattice core construction, including in-plane compression, out-of-plane compression, and bending (Fan *et al.* 2007; Fan *et al.* 2006). In these studies, the panels used metal or FRP components, which in general have significantly different failure mechanisms and generally higher performance characteristics than wood-based materials.

There is no known literature using wood-based materials for the tri-axial rib core structure. Four panel configurations were selected, fabricated, and tested to determine the initial panel properties using standard sandwich panel test methods. The main objective was to evaluate the initial mechanical properties of wood-based sandwich panels with fiberglass faces and foam core and to better understand the mechanical reinforced failure mechanisms of fiberglass and foam for future analyses of these panels.

EXPERIMENTAL

Material Properties

The mechanical properties of the materials used for this study were either obtained from the manufacturer or by testing according to ASTM test methods D638-10 and D695-10. Phenolic impregnated laminated paper of 2.36 mm thickness (NP610 from Norplex-Micarta Inc., Postville, IA) was used for the core and faces. The phenolic resin content is approximately 35%. Laminated paper has orthotropic properties designated as either machine direction (MD) or cross-machine direction (CD) (Table 1).

To achieve slightly higher strength and stiffness for the panel, it was decided to use fiberglass fabric bonded with epoxy no. 635 resin (US Composites Inc., West Palm Beach, Florida) to the outside of the panel. S-fiberglass square woven fabric with a weight of 0.285 kg/m² at a nominal thickness of 0.25 mm was used. During initial fiberglass tensile tests, the fabric failed prematurely by separation between the glass fibers. The test coupons were modified by bonding the fiberglass fabric to the laminated paper and were retested as a combined composite. While the fiberglass had a square weave, the laminated paper/fiberglass composite was tested in the MD and CD directions; Poisson's ratio MD and CD were also obtained from standard tensile tests measuring both axial and transverse strains (Table 1).

Urethane self-expanding foam (US Composites Inc.) was used to fill the core volume between the tri-axial ribs. The expanding foam had a cured density of approximately 48 kg/m³. The epoxy resin was also tested *via* a small dog-bone coupon (Table 1).

Table 1. Component Material Properties

Materials	Density	Comp. strength	Tensile strength MD ^②	Tensile strength CD ^③	MOE MD ^②	MOE CD ^③	Poisson ratio MD	Poisson ratio CD
	(kg/m ³)	(MPa)	(MPa)	(MPa)	(GPa)	(GPa)		
Laminated paper (LP)	1387	241	173.9	118.6	11.6	8.3	0.36	0.27
Fiberglass/L ^①	1310	241	186.3	140.4	12.0	11.4	0.07	0.05
Urethane foam	48	0.41	0.48	-	0.005	-	0.46	-
Epoxy resin	1101	105.9	31.0	-	1.4	-	0.3	-

Note: ① Fiberglass bonded with laminated paper composite. ② MD = mechanical direction.

③ CD = cross direction. ④ Modulus of elasticity.

Fabrication of the Sandwich Panels

Linear ribs were cut from the laminated paper, with the MD of the paper aligned along the length of the ribs. The height of the ribs was nominally 33.0 mm. The slots in the ribs were cut slightly oversized to provide sufficient clearance when assembled (Fig. 1). The distance between all slots was 117.3 mm, creating an equilateral triangle or iso-grid design.

Four panel configurations were constructed (Fig. 2). The first configuration comprised only the tri-axial ribbed core bonded between two faces. The second configuration included additional fiberglass on the outside of both faces. The third configuration included foam between the ribs but without fiberglass. The fourth configuration included both foam and fiberglass.

Liquid expanding urethane foam was poured into the spaces between the ribs before the faces were assembled (Fig. 2b). The inside face surface was lightly sanded prior to applying epoxy resin between the core and face. Light pressure was applied to the faces to maintain a flat surface until the epoxy cured. Then, the outer surfaces were sanded prior to bonding the fiberglass to the faces. The alignment for the fiberglass was square with the MD and CD directions of the paper laminates (Fig. 2c).

Flatwise and edgewise compression tests were conducted on three panel configurations: panels 1, 2, and 3. The dimensions for all the flatwise and edgewise compression specimens are listed in Table 2. The configuration for panel 4 was not used for flatwise compression because it was similar to panel 3 with respect to the foam core support of the ribs, and it was not used for edgewise compression because it was similar to panel 2 for testing the laminate/fiberglass composite in the plane direction. For the edgewise compression tests, two specimens per panel were fabricated and tested, one in the MD and the other in the CD direction of the laminated paper faces and the cores.

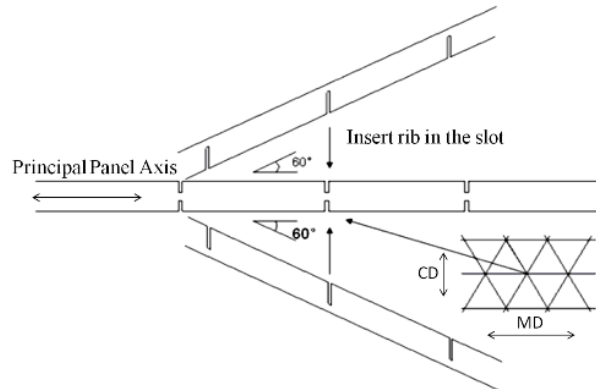


Fig. 1. Fabrication of tri-axial core structure from notched laminates (Li *et al.* 2013)

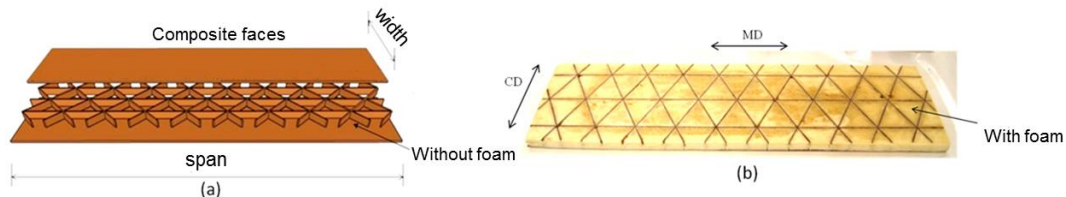


Fig. 2. Wood-based sandwich panels with composite faces and tri-axial core: (a) basic construction of the tri-axial sandwich panel; (b): tri-axial core filled with urethane foam

All four configurations were tested for bending properties. The dimensions for all the bending specimens are listed in Table 2.

The core thickness for panel 4 was slightly thinner than the other three panels due to a need to sand off uneven rib heights that occurred during foam expansion. Similar length and width dimensions were used for all the panels.

Testing Methods

Flatwise compression test

The compressive properties for the core (strength and apparent MOE) were measured using the flatwise compression test ASTM C365-11. The loading rate was 0.5 mm/min. A swivel head was attached to the upper cross-head to reduce any influence of uneven loading due to uneven panel thickness variations. The detailed dimensions for the flatwise compression panels are given in Table 2. Care was exercised to position these dimensions over a specific core arrangement consisting of two complete iso-grid core triangles and rib four intersections.

Table 2. Sandwich Panel Dimensions

Panel ID (No.)	Panel configuration	Density (kg/m ³)	Areal Density (kg/m ²)	Panel load dimensions (mm)	Face thickness (mm)
Flatwise compression test					
1	L ^①	275.3	10.4	254×203×37.8	2.4
2	L+FG ^②	308.7	12.1	254×203×39.1	2.8
3	L+F ^③	334.6	13.0	254×203×38.9	2.4
Edgewise compression test					
1 (MD)	L ^①	275.3	10.4	203×198×37.7	2.4
2 (MD)	L+FG ^②	308.7	11.9	203×198×38.4	2.8
3 (MD)	L+F ^③	334.6	13.0	203×198×38.9	2.4
1 (CD)	L ^①	275.3	10.4	198×203×37.8	2.4
2 (CD)	L+FG ^②	308.7	11.9	198×203×38.6	2.8
3 (CD)	L+F ^③	334.6	13.0	198×203×39.0	2.4
Bending test					
1	L ^①	305.1	11.6	914×267×38.1	2.6
2	L+FG ^②	316.3	12.4	914×267×39.1	3.4
3	L+F ^③	331.2	12.5	914×267×37.8	2.7
4	L+F+FG ^④	397.2	13.8	914×267×34.8	3.5

Note: ① L = laminated paper sandwich panel. ② L+G = laminated paper sandwich panel with S fiber glass coating. ③ L+F = laminated paper sandwich panel with foam filled in the core. ④ L+F+FG = laminated paper sandwich panel with S fiber glass coating and foam filled in the core.

Edgewise compression test

The edgewise compression test ASTM C364-07 was used to measure the in-plane compressive panel strength, face strength, and panel stiffness. A loading rate of 0.5 mm/min was used for the cross-head movement. Two specimens were cut from each panel. One was tested in the MD direction and the other was tested in the CD direction to determine any significant differences in these two directions. The detailed dimensions for the edgewise compression panels are given in Table 2. A swivel head was attached to the upper cross-head to reduce any influence of uneven loading along the edges.

Bending test

The third-point load bending test, ASTM C393-06, was used to measure bending behavior. The width of the panels was determined so that three complete linear ribs were included and centered, as seen in Fig. 2. The span, l , of the simply supported sandwich panel was 914 mm. The panel width, b , was 267 mm. The thicknesses of the faces, t_f , ranged from 2.6 mm without fiberglass to 3.5 mm with it. The total panel thickness, t_p , ranged from 34.8 mm to 39.1 mm, as seen in Fig. 9. The detailed dimensions for the bending panels are given in Table 2.

RESULTS AND DISCUSSION

Mechanical Behavior of Flatwise Compression

The flatwise maximum compression panel stress and rib stress vs. compression strain of flatwise compression are listed in Table 3 and shown in Fig. 3. Failure modes of these sandwich panels are shown in Fig. 4 (a).

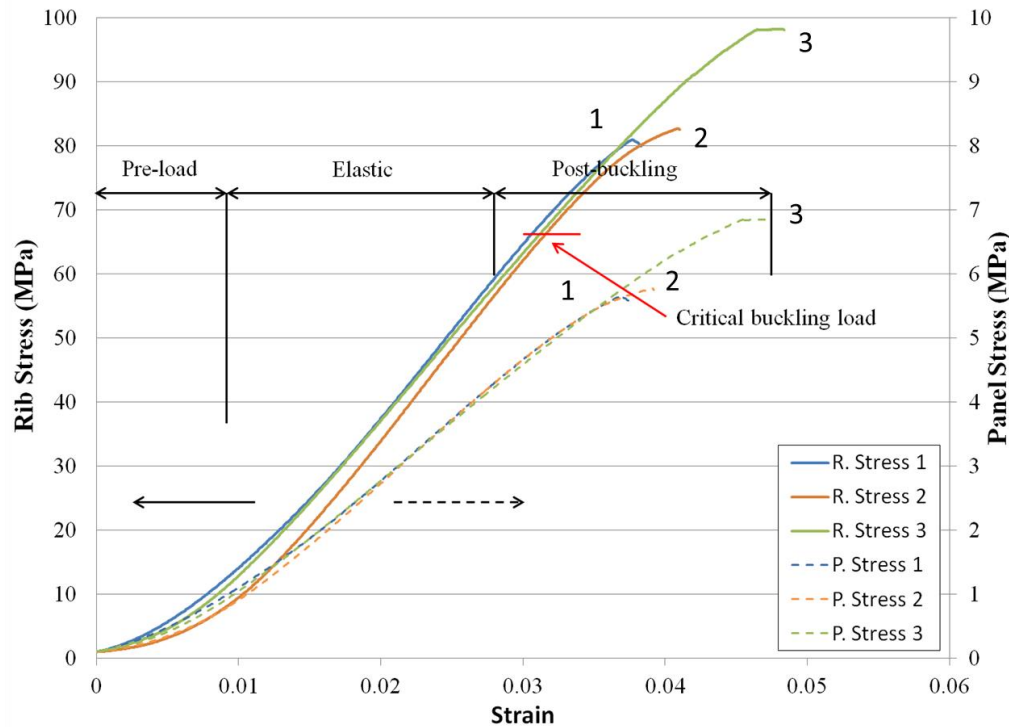


Fig. 3. Flatwise compression stress vs. strain. Panels 1 and 2 are without foam. Panel 3 is the same core configuration with foam.

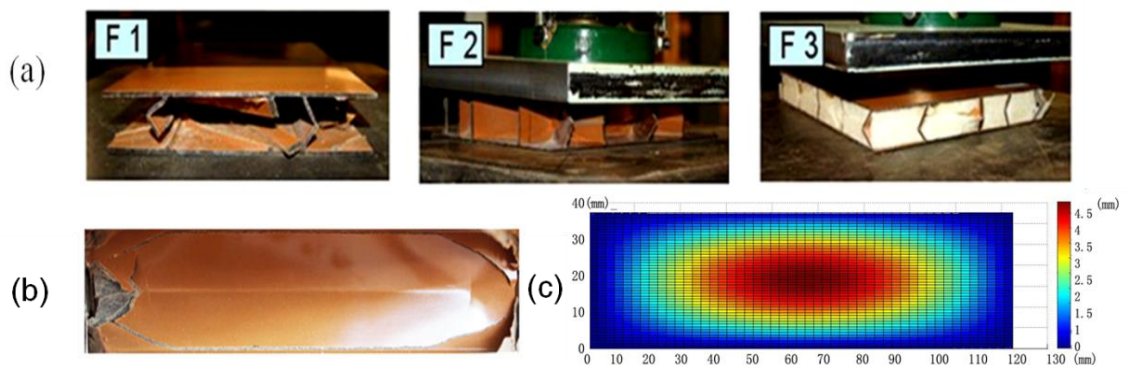


Fig. 4. Typical flat-wise compression failure modes of sandwich panels: (a) typical flat-wise compression failure; (b) the fractures in typical rib buckling failure; (c) out-of-plan displacement at buckling for each rib without foam

Examination of panels 1 and 2 showed that the ribs in the core had brittle failure in post-buckling after buckling at loads of 291 kN and 298 kN, respectively. As expected, the fiberglass fabric on the faces did not have any noticeable effect on flatwise

compression performance. However, for panel 3, similar buckling behavior of the ribs still occurred (Fig. 3), but the foam did provide partial lateral restraint to resist initial out-of-plane buckling,

$$F_z^{fcu} = \frac{P_{max}}{A} \quad (1)$$

where P_{max} denotes the maximum load and A is the cross section area of the panel. Maximum panel stresses, F_z , for panels 1, 2, and 3 were 5.65 MPa, 5.77 MPa, and 6.85 MPa, respectively. The flatwise compression stress supported by the tri-axial ribs can be calculated using Eq. 2,

$$\sigma_r = \frac{P_{max}}{A_r} \quad (2)$$

where A_r is the total cross section of the tri-axial ribs. The maximum strengths of the ribs in the core for panels 1, 2, and 3 were 80.9 MPa, 82.7 MPa, and 98.2 MPa, respectively.

The maximum stress capacity for the foam was 0.41 MPa, which was less than 0.2% of that of the ribs, and its apparent MOE was 0.04% of that of the laminated paper. The foam was 93% of the total area and could probably support about 11.7 kN or about 7% of the total load of 354 kN for panel 3. The foam did not add significantly to the MOE, yet for panel 3, the foam improved the ultimate stress by 18%. The apparent MOE for panels 1, 2, and 3 were similar, at 0.16 GPa, 0.18 GPa, and 0.18 GPa, respectively. The MOE values were calculated prior to buckling; thus, their predominant effects were due to the laminate core prior to buckling and not due to the foam. The foam helped to delay the initial onset of rib buckling; however, it was not enough to keep the rib from buckling. The maximum rib compression stress for the laminate paper was 241 MPa, given in Table 3, which was not achieved in the test due to the buckling failure. It is probable that a stiffer foam could have been used to provide even more support to the ribs and thus achieve even higher stress and stiffness through-the-thickness.

The flatwise compression data revealed a non-linear relationship between stress and strain, as can be seen in Fig. 3, especially at the beginning and at the end. The non-linear behavior at the beginning can be attributed to a slight “settling-in” for the test equipment and between the faces and core ribs. The modulus of the epoxy is about 10% that of the ribs. The mid-linear portion of the data represented between 25% to 75% of the ultimate strain for panels 1 and 2, and was between 20% and 60% of the ultimate strain for panel 3. Toward the end of the linear variation phase, the stress *versus* strain of each panel showed non-linear behavior due to the critical buckling of the ribs, until brittle fracture occurred.

The critical buckling load was estimated from the governing differential equation based on the orthotropic laminate plate theory shown in Eq. 3 (Vinson 1999),

$$D_{11} \frac{\partial^4 w}{\partial x^4} + 2(D_{12} + 2D_{66}) \frac{\partial^4 w}{\partial x^2 \partial y^2} + D_{22} \frac{\partial^4 w}{\partial y^4} = N_x \frac{\partial^2 w}{\partial x^2} + 2N_{xy} \frac{\partial^2 w}{\partial x \partial y} + N_y \frac{\partial^2 w}{\partial y^2} \quad (3)$$

where w is the buckling deformation in the out of plane direction, and D_{11} , D_{12} , D_{22} , and D_{66} are the bending-twisting stiffness moduli of the orthotropic laminate plate. Because of the total buckling failure of the sandwich panels shown in Fig. 4 (a), it was assumed that the load transferred to the ribs uniformly, and the panels were analyzed for critical

buckling load or buckling stress (Fig. 4b, c). The foam can improve maximum flatwise compression strength by partially restraining out-of-plane deformation during the pre-buckling phase. However, the foam had limit domination to the compression strength. Due to the current foam's low stiffness, the same critical buckling load could be used as those without the foam. Therefore, it was ignored in the calculation of rib critical buckling stiffness as compared with the laminated paper (Table 1). Fracture cracks were observed around the perimeter of the rib (Fig. 4b). For our analyses, the boundary conditions were assumed as rigidly supported; then, the buckling mode shapes can be given as in Eq. 4,

$$w_{mn} = \sum_{m=1}^{\infty} \sum_{n=1}^{\infty} A_{mn} \sin \frac{m\pi x}{a} \sin \frac{n\pi y}{b} \quad (4)$$

where A_{mn} is the arbitrary amplitude coefficient and m and n are the half wave in the x and y directions, respectively. The estimated deformation pattern (Fig. 4c), was similar to the actual failure mode of the ribs shown in Fig. 4b.

Based on the Bubnov-Galerkin method and boundary conditions (Brukva 1968), the critical buckling load, N_{xcr} , can be determined from Eq. 5,

$$N_{xcr} = \sigma_{cr} t = -\frac{0.96\pi^2}{b^2} \left[3.25 \left(\frac{D_{11}}{D_{22}} \right)^{\frac{1}{2}} + 2.67(D_{12} + 2D_{66}) + 4.92 \left(\frac{D_{11}}{D_{22}} \right)^{\frac{3}{2}} \right] \quad (5)$$

where a is the length of the plate (rib section length), b is the width of the plate (rib height), and t is the thickness of the rib. Both m and n are equal to 1 according to the buckling failure mode. The bending-twisting stiffness moduli are calculated by material properties (Brukva 1968). From Eq. (5), the critical buckling stress was estimated to be 66.5 MPa (Fig. 5), consistent with the values observed for the critical buckling stress for panels 1, 2, and 3, where the non-linear behavior starts toward the end of the curves. The foam limited the initial out-of-plane displacement enough to slightly increase the flatwise compression load, but still less than if the full compressive stress of 241 MPa were developed for full failure load in rib compression (Table 1).

The authors believe that improved flat-wise panel compression properties are possible with thicker ribs that fail in compression rather than buckling or with smaller iso-grid equilateral triangle tri-axial size to decrease the equivalent stress in the rib σ_r . Also, stiffer foam in the core could improve the resistance to buckling in flat-wise compression. There may be applications where buckling would be the preferred method of failure, such as for cushioning and impacting applications. For these situations, buckling stress and load values would be necessary; these values could be estimated and engineered.

Mechanical Behavior of Edgewise Compression

The edgewise compression face stress and panel stress vs. strain results are listed in Table 3 and are shown in Figs. 5 and 6 for the MD and CD directions, respectively. The labels marked F.Stress 1, F.Stress 2, and F.Stress 3 represent the face stress for panels 1, 2, and 3, respectively. The labels marked P.Stress 1, P.Stress 2 and P.Stress 3 represent the panel stress for panels 1, 2, and 3, respectively. The MD panels had two linear ribs aligned parallel to the loading direction, while the CD panels had two

linear ribs oriented perpendicular to the loading direction; see Fig. 2 (a). According to ASTM C364-07, the face stress of edgewise compression tests can be calculated as,

$$\sigma_f = \frac{P}{(w \times 2t_{fs})} \quad (6)$$

where P is load, w is the width of panel, and t_{fs} is the thickness of a single face.

The panel stress for the edgewise compression tests can be calculated by,

$$\sigma_p = \frac{P}{(w \times t_p)} \quad (7)$$

where t_p is the thickness of the panel.

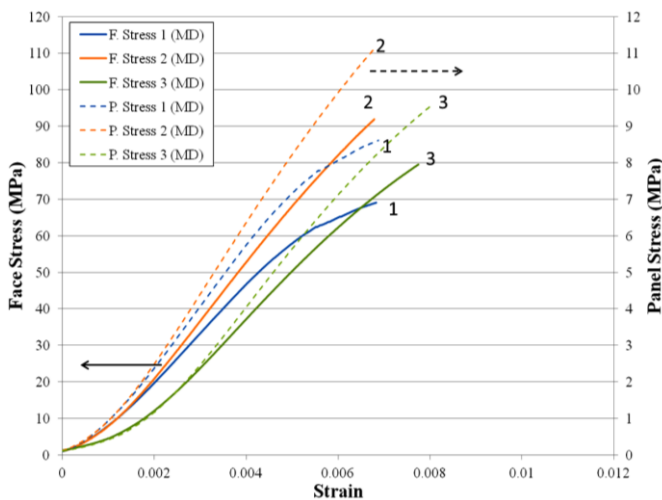


Fig. 5. Edgewise compression face stress (F. Stress) and panel stress (P. Stress) vs. strain in the machine direction

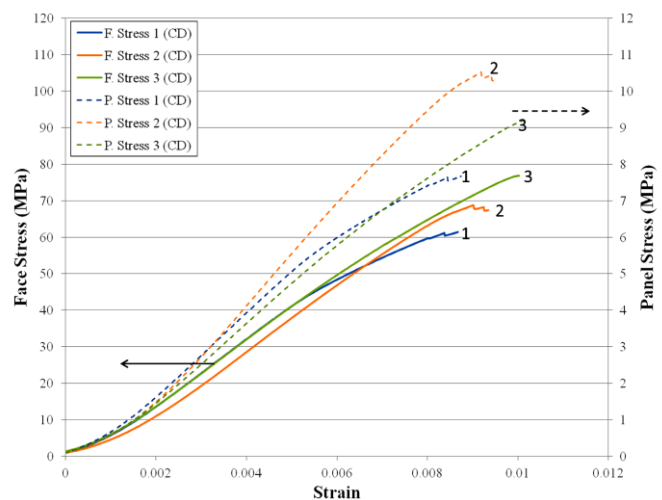


Fig. 6. Edgewise compression face stress (F. Stress) and panel stress (P. Stress) vs. strain in the cross-machine direction

From Table 3, the maximum panel load among the MD panels was exhibited by panel 2 (with fiberglass), at 87.0 kN, followed by 75.2 kN and 65.0 kN for panels 3 and 1, respectively. Similarly, for the CD panels, the highest panel load was 84.4 kN for panel 2, followed by panels 3 and 1 at 74.5 kN and 59.3 kN, respectively. The fiberglass increased the thickness by about 10%, which helped to stiffen the faces. Figure 7a without fiberglass shows severe buckling, whereas Fig. 7c still shows some buckling, yet not as much as panel 1, resulting in higher loads before face-buckling developed. The foam for panel 3 helped support the faces, (Fig. 7e), but the fiberglass for panel 2, which is a stiffer material, helped to increase the in-plane stiffness (equal apparent MOE multiplied effective area) (Figs. 5 and 6); hence, the slopes of the panel apparent MOE in the MD and CD directions were higher for the fiberglass panel, panel 2 (Table 3). The foam panel 3, helped to prevent out-of-plane displacement and helped prevent buckling, thus increasing the failure load compared with panel 1. Both the fiberglass and foam panels had almost linear stress vs. strain responses, while panel 1 (MD), without fiberglass, showed non-linear buckling curvature toward failure. Panel apparent MOE for panel 2 in the MD and CD directions were over 10% greater than the panels without fiberglass fabric (panel 1) and with foam (panel 3) (Table 3). Panel apparent MOE for the

panels with and without foam were similar and should be, as measurement of the modulus was done before buckling and the dominant material was the laminated paper. The foam restrained the faces, but its stiffness was not sufficient to add much to the total panel apparent MOE. The apparent MOE for the MD direction were about 30% greater than those in the CD direction. This is better than the 40% difference for the MD material properties over the CD properties. It is possible that the ribs may have helped stiffen the panel, but this will need more investigation in another study to determine the effect of rib orientation on the performance of the panel.

Table 3 shows the specific apparent MOE, which is the ratio of panel apparent MOE and areal density. The results indicate that foam filled in the core was 0.123 GPa·m²/kg in MD and 0.092 GPa·m²/kg in CD. The foam did not increase the specific MOE compared with panel without foam, because most of the foam in the core was not sufficient to significantly increase the compression properties. By contrast, the fiberglass coating in the faces increased the stiffness of the faces, which improved the edgewise specific MOE. However, for the flatwise compression testing, the faces had no contribution for the panels with or without fiberglass had same values of specific MOE, which was 0.015 GPa·m²/kg for both panels with and without fiberglass.

MD direction face stress for panel 2 was maximum, followed by panel 3 and panel 1 (Figs. 5 and 6; Table 3). Maximum face stress in the CD direction was for panel 3, followed by panels 2 and panel 1. For both orientations, only the face area was used to determine face stress; however for the MD panels there were 2 ribs aligned in the loading direction, which may have contributed to the higher loads and higher calculated stresses (Fig. 7b). On the other hand, the ribs in the CD loading direction were off-axis (Fig. 7d), and may not have had much influence on the maximum load, thus contributing to a lower calculated face stress. Also, the MD vs. CD orientation of the faces can contribute to in-plane buckling results due to the stiffness differences between the two directions. More study needs to be done to determine the effects of buckling as a function of the core rib spacing and orientation. The foam helped prevent face buckling, even without the addition of fiberglass.

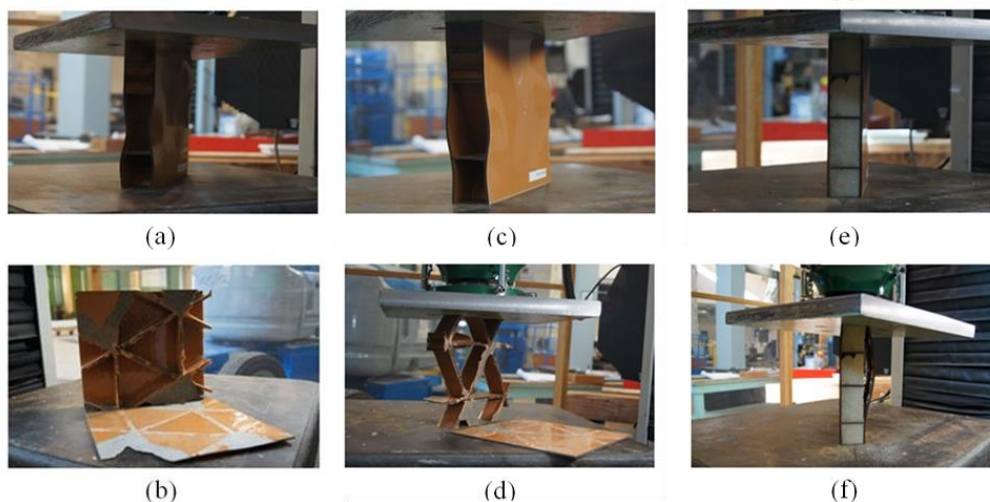


Fig. 7. The failure modes for edgewise compression tests: (a) and (b) face buckling followed by face delamination failure modes for the laminated paper-only panel; (c) and (d) face buckling followed by face delamination failure modes for the fiberglass/laminated paper panel; (e) and (f) concave face buckling reduced by the foam and delamination failure modes for the foam/laminated paper panel

The primary failure mode for edgewise compression tests was buckling of the faces between the ribs, so that shear failure between the faces and core was not evident. Figure 7 (a), (c), and (e) show the buckling conditions of laminated paper faces. In the edgewise test, the face pre-buckling with small out-of-plane deformation occurred at around 30 to 40% of failure load by the observation. As the load increased, face buckling gradually developed within the triangular cell boundary up to failure. The failure occurred at the central section of sandwich panel faces where the faces debonded from the ribs, as can be seen in Fig. 7f. The sandwich panel with fiberglass reinforced the face stiffness, reducing the face lateral deformation during the buckling phase. Therefore the buckling load was higher than without the fiberglass coating. Foam also could prevent the lateral deformation. However, due to the foam's low stiffness, the effect of reinforcement was less than fiberglass coating for delaying face buckling. It is believed that shortening the span of the ribs or increased stiffness of the faces through material properties or thickness would reduce buckling of the faces in edge compression

Table 3. Flatwise and Edgewise Compression Test Results

Panels ID (No.)	Comp. failure load (kN)	Panel apparent MOE ^① (GPa)	Specific panel MOE ^② (GPa·m ² /kg)	Ultimate panel stress (MPa)	Ultimate rib stress (MPa)	Ultimate face stress (MPa)
Flatwise compression test						
1	291	0.16	0.015	5.65	80.9	-
2	298	0.18	0.015	5.77	82.7	-
3	354	0.18	0.014	6.85	98.2	-
Edgewise compression test						
1 (MD)	65.0	1.6	0.154	8.6	-	69.3
2 (MD)	87.0	1.8	0.152	11.2	-	81.7
3 (MD)	75.2	1.6	0.123	9.57	-	78.1
1 (CD)	59.3	1.2	0.115	7.7	-	61.6
2 (CD)	84.4	1.4	0.117	10.3	-	75.5
3 (CD)	74.5	1.2	0.092	9.2	-	75.4

Note: ① Panel apparent MOE is modulus of elastic on 20%-40% slope of panel. ② Specific MOE is the ratio of panel apparent MOE and areal density.

Mechanical Behavior of Bending

The bending load and face stress vs. deflection curves are shown in Fig. 8 and listed in Table 4. The panel bending failure loads were 10.1 kN, 18.2 kN, 12.1 kN, and 15.1 kN, respectively. The peak loads for the fiberglass panels 2 and 4 were higher than for panels 1 and 3 without fiberglass. The failure load for panel 2, with fiberglass, was 82% higher than panel 1 without foam. The load/deflection curve for panel 4 was also higher than panel 3. However, panel 4 was significantly less than panel 2; this was because the panel was physically thinner. The ribs for panel 4 not as high because they were sanded prior to bonding the faces onto the core because of uneven core rib height alignment due to the foam expansion and movement of the ribs as the foam set. If panel 4 were of similar thickness, then one would have expected a slightly higher failure load/deflection curve than that of panel 2 because both the fiberglass and the foam provided additional support to the faces and ribs. Figure 8 also shows plots of face stress

vs. deflection. It is believed localized rib buckling failure occurred in the panels prior to achieving failure tensile or compressive stress due to observed rib failure.

The bending failure modes for each panel are shown in Fig. 9. The failure modes of panels 1 and 2, without foam, were buckling failure near the top faces, compared with the shear failure in the core for panels 3 and 4, with foam and fiberglass. For panels 1 and 2, as the load increased, the top face began to buckle out-of-plane between the rib spaces. Failure was similar to the edgewise compression out-of-plane behavior shown in Fig. 7 (a) and (c). Furthermore, the ribs for panels 2 exhibited buckling/compression failure from the compression under the upper face at the loading points. For panels 3 and 4, with foam, both panel failures involved shear strength failure between the rib:face bond interface between the loading points in the mid-section. The rib:face bonding strength was not sufficient to hold the panel faces in-place to achieve the full face compression stress listed in Table 1. At failure, the bottom faces were suddenly ruptured. The failure load of panel 4 with fiberglass was 15.1 kN, 24.8% higher than that of panel 3, even with the thinner section.

From post observation of the failed panels, it is believed that one of the reasons the panels with foam did not reach maximum potential load was because the foam may have absorbed some of the adhesive into the open foam cells next to the ribs rather than its being used between the rib:face interface, thus decreasing joint performance. There was significant resin failure as compared to the paper laminate failure in panels 1 and 2. However, the foam did help resist concave deflection of the faces into the open rib spaces and did provide better support under the load points to help prevent compressive rib failure (Fig. 9a, b vs. c, d).

Comparing panel 2 with panel 4, both panels have fiberglass, which significantly increased the compression/tensile stress capacity. Also, the face thickness for both panels was increased, which increase face stiffness and helped reduce the buckling behavior of the faces between the ribs. The maximum strain for the panels, Eq. (8), can be estimated using the deflection, Δ . Thus, the stress was calculated using Young's modulus from Table 1,

$$\varepsilon = \frac{12\Delta h}{L^2(3-(1-\frac{a}{L})^2)}, \quad \sigma = E\varepsilon \quad (8)$$

where ε is the strain at the center point of the panel, Δ is the maximum deflection, L is the span, and a is the distance from the reaction to nearest load point. The experimental stress can be estimated from the maximum face strain. Similarly, using Eq. (9) from ASTM C393-06, the maximum face stress from bending can be calculated, but this assumes no contribution from the core. This equation is calculated as a reference value at maximum applied force and given by,

$$\sigma_f = \frac{P_{max}l}{3t(d+c)b} \quad (9)$$

where σ_f denotes the maximum face bending stress, P_{max} is the maximum bending load, and d is the sandwich thickness. The results from Eqs. (8) and (9) are listed in Table 4. Panels 2 and 4 were able to carry larger stresses in bending than panels 1 and 3. Foam also improved the bending performance, but it was not sufficient to resist the high shear

stress at the rib:face interface. The panels were also compared based on bending rigidity, EI . The actual EI values from the tests were determined from Eq. 10,

$$EI = \frac{\text{Slope} \cdot a}{48} (3l^2 - 4a^2) \quad (10)$$

where slope is the ratio of the load to the maximum deflection based on the regression results; l and a represent the span of the sandwich panel and the distance from the outside support to the load point, respectively.

The contribution to the total panel stiffness from the faces was significantly higher than the contribution from the tri-axial core. The theoretical rigidity $(EI)_{eq}$ of the sandwich panel without a core is given by (Allen 1969),

$$(EI)_{eq} = \frac{E_f b t c^2}{2} \quad (11)$$

where E_f is the elastic modulus of the faces, symbols b , t , and c represent the panel width, face thickness, and core height, respectively. The results of bending rigidity EI and theoretical rigidity $(EI)_{eq}$ are listed in Table 4. The measured bending rigidity value of panel 2 was the highest, at $7.52 \text{ kN}\cdot\text{m}^2$, followed by panel 3 at $6.09 \text{ kN}\cdot\text{m}^2$, panel 4 at $6.00 \text{ kN}\cdot\text{m}^2$, and panel 1 at $5.59 \text{ kN}\cdot\text{m}^2$. This indicates that the bending rigidity of the panels was increased by approximately 25% using fiberglass (panel 3) and approximately 10%, using foam (panel 2), both compared to panel 1. The thickness of panel 3 was greater than that of panel 4. The bending rigidity of panel 3 with foam was only a little higher than that of panel 4, with both foam and fiberglass, because the sandwich panel thickness was greater. The theoretical rigidity values for each panel show that the maximum predicted rigidity value for panel 2 was $5.65 \text{ kN}\cdot\text{m}^2$, followed by panel 3 at $5.02 \text{ kN}\cdot\text{m}^2$, panel 4 at $4.35 \text{ kN}\cdot\text{m}^2$, and panel 1 at $4.28 \text{ kN}\cdot\text{m}^2$. Comparing the tested bending rigidity results with the theoretical rigidity results, the predicted rigidities of the panels were 17.6% to 24.8% less than the tested values. The theoretical rigidity values assumed that the core had no effect on the performance, but in fact, the core significantly influenced the bending performance.

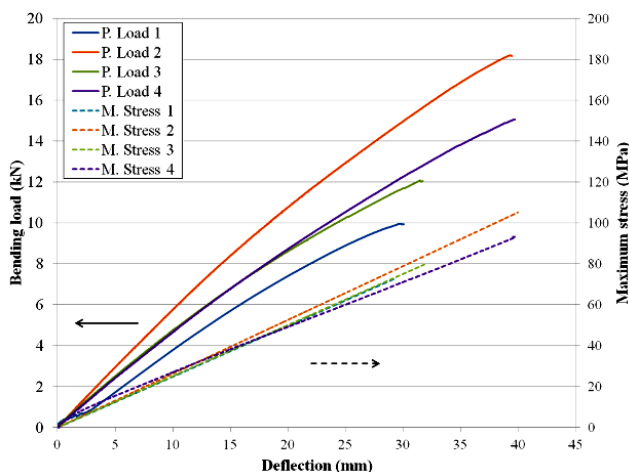


Fig. 8. The bending results for loading and deflection on each specimen

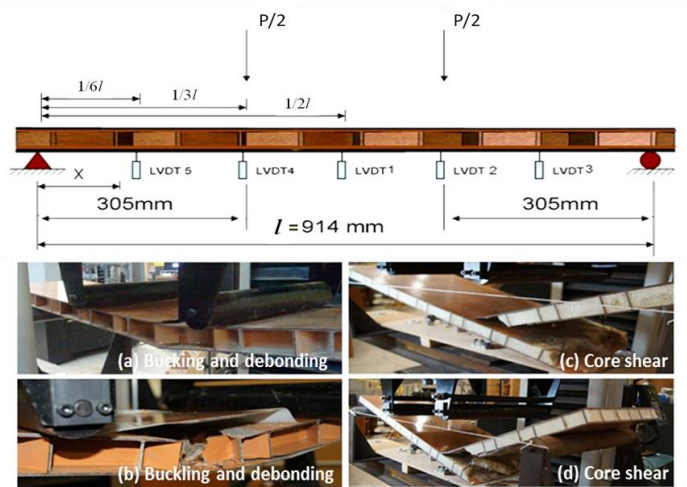


Fig. 9. The bending test setup and failure modes

Table 4. Sandwich Panel Bending Test Results and Comparison between Actual and Theoretical Panel Rigidity

Panels ID (No.)	Failure load (kN)	Experimental stress (MPa)	Face bending stress ASTM C393-06 (MPa)	Bending rigidity EI (kN.m ²)	Theoretical rigidity (E) _{eq} (kN.m ²)
1	10.0	73.1	94.5	5.59	4.28
2	18.2	103.6	129.3	7.52	5.65
3	12.1	78.8	93.7	6.09	5.02
4	15.1	93.2	116.8	6.00	4.35

CONCLUSIONS

1. In flatwise compression, the compression load was carried by the tri-axial ribbed core. Fiberglass fabric bonded on the outside faces had no noticeable effect on the flatwise compression properties. However, the foam filled core helped resist rib buckling, which increased the rib compression strength. A stiffer foam should be recommended to better support the faces and also to help prevent lateral rib buckling. To improve the flatwise compression properties, it is possible to engineer the foam for both structural as well as cushioning and any impact applications. Thicker ribs or shorter rib spacing could be used increase flatwise compression strength.
2. In edgewise compression, face buckling was the primary failure mode. The fiberglass significantly reinforced the edgewise compression properties by increasing the stiffness of the faces. The foam also contributed to the reduction of concave buckling of the faces into the core between the ribs during the post-buckling phase. Failure occurred at the central section of sandwich panel faces where the faces debonded from the ribs. Either additional fiberglass fabric or higher stiffness foam or both could be used to improve the mechanical properties during edgewise compression. Additional support of the faces with decreased rib spacing would reduce face buckling and increase edgewise compression strength.
3. In third-point load bending, the fiberglass and foam were shown to improve the bending properties of the sandwich panel. It is possible that the foam may have absorbed some of the epoxy into its open foam cells, preventing the epoxy from adequately bonding the ribs to the faces and thus reducing the potential load-carrying capacity. We believe that if foam were injected into the core after bonding the core to the faces, it would have yielded higher bending properties. The experimental and theoretical results of bending rigidity show that the stiff core had a significant effect on the bending performance. Therefore, the mechanical influence of the core for sandwich panels should be considered in the design.

ACKNOWLEDGMENTS

This work was supported by the USDA, Forest Products Laboratory; the authors gratefully acknowledge the support of Sara Fishwild, James Bridwell, Marshall Begel, Tim Nelson, Dave Simpson, and Marc Joyal of the EMRSL group for the mechanical testing. Tim Scott and Jane O'Dell are thanked for editorial comments.

REFERENCES CITED

- Allen, H. G. (1969). *Analysis and Design of Structural Sandwich Panels*, Pergamon Press, Oxford.
- Aviles, F., and Carlsson, L. A. (2006). "Three-dimensional finite element buckling analysis of debonded sandwich panels," *Journal of Composite Materials* 40(11), 993-1008.
- Brukva, N. F. (1968). "Stability of rectangular orthotropic plates," *Prikladnaya Mekhanika* 4(3), 77-85.
- Chen, H. J., and Tsai, S. W. (1996). "Analysis and optimum design of composite grid structures," *Journal of Composite Materials* 30(4), 503-534.
- Davalos, J. F., Qiao, P. Z., Xu, X. F., Robinson, J., and Barth, K. E. (2001). "Modeling and characterization of fiber-reinforced plastic honeycomb sandwich panels for highway bridge applications," *Composite Structures* 52(3), 441-452.
- Evans, A. G., Hutchinson, J. W., Fleck, N. A., Ashby, M. F., and Wadley, H. N. G. (2001). "The topology design of multifunctional cellular metals," *Progress in Materials Science* 46(3), 309-327.
- Fan, H. L., Meng, F. H., and Yang, W. (2007). "Sandwich panels with kagome lattice cores reinforced by carbon fibers," *Composite Structures* 81(4), 533-539.
- Fan, H. L., Meng, F. H., and Yang, W. (2006). "Mechanical behaviors and bending effects of carbon fiber reinforced lattice materials," *Archive of Applied Mechanics* 75(10-12), 635-647.
- Han, D. Y., and Tsai, S. W. (2003). "Interlocked composite grids design and manufacturing," *Journal of Composite Materials* 37(4), 287-316.
- Hunt, J. F., Harper, D. P., and Friedrich, K. A. (2004). "Three-dimensional engineered fiberboard: Opportunities for the use of low valued timber and recycled material," *38th International Wood Composites Symposium Proceedings*, Pullman, WA, pp. 207-216.
- Johnsson, H., Blanksvärd, T., and Carolin, A. (2006). "Glulam members strengthened by carbon fibre," *Materials and Structures* 40(1), 47-56.
- Li, J. H., Hunt, J. F., Cai, Z. Y., and Zhou, X. Y. (2013). "Bending analyses for 3D engineered structural panels made from laminated paper and carbon fabric," *Composites Part B* 53, 17-24.
- Plevris, N., and Triantafillou, T. (1992). "FRP-reinforced wood as structural material," *Journal of Materials in Civil Engineering* 4(3), 300-317.
- Sharaf, T., and Fam, A. (2011). "Experimental investigation of large scale cladding sandwich panels under out-of-plane transverse loading for building applications," *Journal of Composites for Construction* 13(3), 422-430.

- Taczala, M., and Banasiak, W. (2004). "Buckling of I-core sandwich panels," *Journal of Theoretical and Applied Mechanics* 42(2), 335-348.
- Vinson, J. R. (1999). *The Behavior of Sandwich Structures of Isotropic and Composite Materials*, Technomic Publishing Company, Lancaster, PA.
- Vasiliev, V. V., Barynin, V. A., and Rasin, A. F. (2001). "An isogrid lattice structures survey of development and application," *Composite Structures* 54(2), 361-370.
- Wei, X., Tran, P., De Vaucorbeil, A., Ramaswamy, R. B., Latourte, F., and Espinosa, H. D. (2013). "Three-dimensional numerical modeling of composite panels subjected to underwater blast," *Journal of the Mechanics and Physics of Solids* 61(6), 1319-1336.
- Zhang, Y. H., Qiu, X. M., and Fang, D. N. (2008). "Mechanical properties of two novel planar lattice structures," *International Journal of Solids and Structures* 45(13), 3751-3768.

Article submitted: November 6, 2013; Peer review completed: January 6, 2014; Revised version received and accepted: January 31, 2014; Published: February 7, 2014.